

REPORT DOCUMENTATION PAGE			Form Approved OMB NO. 0704-0188	
<small>Public reporting burden for this collection of information is estimated to average 1 hour per response, including the time for reviewing instructions, searching existing data sources, gathering and maintaining the data needed, and completing and reviewing the collection of information. Send comment regarding this burden estimate or any other aspect of this collection of information, including suggestions for reducing this burden, to Washington Headquarters Services, Directorate for Information Operations and Reports, 1215 Jefferson Davis Highway, Suite 1204, Arlington, VA 22202-4302, and to the Office of Management and Budget, Paperwork Reduction Project (0704-0188), Washington, DC 20503.</small>				
1. AGENCY USE ONLY (Leave blank)		2. REPORT DATE 07/30/01		3. REPORT TYPE AND DATES COVERED Final Report 07/01/98-06/30/01
4. TITLE AND SUBTITLE Improved Modeling of Drop Vaporization and Combustion in Diesel Sprays			5. FUNDING NUMBERS DAAG55-98-1-9442	
6. AUTHOR(S) John Abraham				
7. PERFORMING ORGANIZATION NAMES(S) AND ADDRESS(ES) Purdue University, Purdue Research Foundation West Lafayette, IN 47907			8. PERFORMING ORGANIZATION REPORT NUMBER 530 1288 1549/FINAL	
9. SPONSORING / MONITORING AGENCY NAME(S) AND ADDRESS(ES) U.S. Army Research Office P.O. Box 12211 Research Triangle Park, NC 27709-2211			10. SPONSORING / MONITORING AGENCY REPORT NUMBER P-37761-EG 8	
11. SUPPLEMENTARY NOTES The views, opinions and/or findings contained in this report are those of the author(s) and should not be construed as an official Department of the Army position, policy or decision, unless so designated by other documentation.				
12a. DISTRIBUTION / AVAILABILITY STATEMENT Approved for public release; distribution unlimited.			12 b. DISTRIBUTION CODE 20010831 041	
13. ABSTRACT (Maximum 200 words) In this work, multicomponent and single component droplet vaporization characteristics are investigated by employing computational models. It is shown that simplified droplet vaporization models that do not solve temperature gradients or flow within the droplet and do not solve gradients in temperature or species in the immediate surrounding of the droplet are able to reproduce droplet vaporization rates and droplet lifetimes with about 15% accuracy compared to detailed models for typical Diesel operating conditions. Under high temperature (> 1200 K) conditions the differences begin to increase. However, it is also shown that under such conditions as well as at even lower temperatures (> 900 K) the vaporization process is mixing limited. i.e., the droplet lifetime is not controlling but rather the characteristic time for mixing of ambient air with the vapor phase the liquid, vapor and air are in phase equilibrium. It is shown that droplets are not likely to reach the critical state under typical engine conditions. With application to multidimensional spray models as focus, a new model for predicting the outcome of drop collisions has been developed. Such models are important because they predict the drop sizes in the spray following atomization.				
14. SUBJECT TERMS			15. NUMBER OF PAGES 27	
			16. PRICE CODE	
17. SECURITY CLASSIFICATION OR REPORT UNCLASSIFIED		18. SECURITY CLASSIFICATION OF THIS PAGE UNCLASSIFIED		19. SECURITY CLASSIFICATION OF ABSTRACT UNCLASSIFIED
			20. LIMITATION OF ABSTRACT UL	

MEMORANDUM OF TRANSMITTAL

U.S. Army Research Office
ATTN: AMSRL-RO-BI (TR)
P.O. Box 12211
Research Triangle Park, NC 27709-2211

☐ Reprint (Orig + 2 copies)

☐ Technical Report (Orig + 2 copies)

☐ Manuscript (1 copy)

☒ Final Progress Report (Orig + 2 copies)

☐ Related Materials, Abstracts, Theses (1 copy)

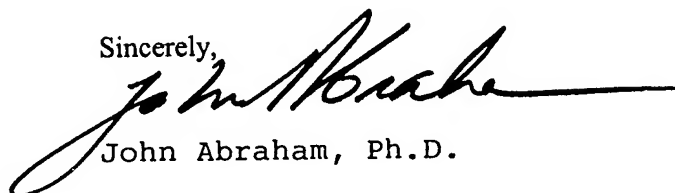
CONTRACT/GRANT NUMBER: DAAG55-98-1-9442

REPORT TITLE: Improved Modeling of Drop Vaporization and Combustion
in Sprays

is forwarded for your information.

SUBMITTED FOR PUBLICATION TO (applicable only if report is manuscript):

Sincerely,



John Abraham, Ph.D.

Enclosure 3

FORECAST EXPENDITURE REPORT
(IMPORTANT!>>>YOU MUST REPLY TO RECEIVE ADDITIONAL FUNDING<<<)

The research agreement identified below is under consideration for additional funding. The contemplated funding, resulting in an extension to the performance period of the agreement, is consistent with the terms and conditions of the agreement. Before a decision can be made to provide the additional funding, the following information is needed: (i) an

IMPROVED MODELING OF DROP VAPORIZATION AND COMBUSTION IN SPRAYS

Final Progress Report

ARO Contract Number: DAAG55 – 98 – 1 – 9442

Principal Investigator:

**John Abraham, Ph.D.
Associate Professor
Maurice J. Zucrow Laboratories
School of Mechanical Engineering
Purdue University
West Lafayette, In 47907-1003**

Table of Contents

Foreword	4
Statement of the Problem Studied	5
Summary of the Most Important Results	6
The Computational Model	6
The One-Dimensional Droplet Vaporization Model	6
Simplified Droplet Vaporization Model	8
Discussion of Results	14
Summary	17
Table 1	19
Figures	20

List of Tables and Illustrations

Table 1. Critical Constants of Pure Fluids.

Figure 1. Schematic of model formulation.

Figure 2. Computational domain and grid for (a) detailed single droplet, (b) single droplet employing multidimensional model and (c) multidimensional spray computations.

Figure 3. Size histories of n-hexadecane droplets.

Figure 4. Size histories of n-hexadecane droplets.

Figure 5. Drop temperature as a function of time.

Figure 6. Size history of n-hexadecane droplet.

Figure 7. Drop temperature as a function of time.

Figure 8. Size histories of n-hexadecane droplets vaporizing in nitrogen at 50 atm.

Figure 9. Size history of n-hexadecane droplet vaporizing in nitrogen at 50 atm and 1300K.

Figure 10. Surface temperatures of n-hexadecane droplets vaporizing in nitrogen at 50 atm.

Figure 11. Critical loci for droplets vaporizing in nitrogen environments.

Figure 12. Normalized mass vaporization rate of a 245 μm C6/C16 (50/50 by mass) droplet vaporizing in nitrogen.

Figure 13. Variation of drop size with time for droplet ambient with same initial temperature of 1400K but different pressures.

Figure 14. Variation of drop size with time for droplet in ambient with same initial pressure of 48 atm but different temperatures.

Figure 15. Computed SMD for 10,000 parcels uniformly distributed throughout a $5 \times 5 \times 0.5$ cm domain at 300K, 1.16 kg/m^3 . 1000 drops per parcel. Brazier-Smith et al., (1972) coalescence model employed.

Figure 16. Computed SMD for 10,000 parcels uniformly distributed throughout a $5 \times 5 \times 0.5$ cm domain at 300K, 1.16 kg/m^3 . 100 drops per parcel. Brazier-Smith et al., (1972) and composite models are compared.

Figure 17. Computed SMD for 10,000 parcels uniformly distributed throughout a $5 \times 5 \times 0.5$ cm domain at 300K, 1.16 kg/m^3 . 100 drops per parcel. Grid resolution is 40×40 cells.

Foreword

This is a study in the general area of multidimensional modeling of Diesel sprays. In this work, the vaporization and combustion characteristics of droplets in a Diesel engine are studied computationally. It has been determined that individual 'droplet' combustion is not relevant in Diesel engines. The vaporization rate determines the rate at which vapor fuel becomes available for mixing and burning. It also determines whether the liquid impinges on the walls of the cylinder. Such impingement is undesirable. The work is carried out from the point of view of applications to modeling sprays in Diesel engines. Hence, it focuses not just on vaporization rates of droplets but on determining these drop sizes since the sizes are the most important parameter in determining vaporization. The droplet modeling studies are integrated with studies of modeling Diesel sprays.

Statement of the Problem Studied

Typical liquid injection velocities in a Diesel engine are over 400 m/s. With such high velocities, the liquid fuel atomizes into droplets of sizes of 0(1)-0(10) μm [1-4]. The chamber gas temperature and pressure under warm operating conditions are in the range of 900-1100 K and 70-120 bars respectively, whereas under cold-start conditions they are 700-900 K and 40-70 bars respectively. The wide range of drop sizes and thermodynamic conditions in the engine chamber makes it necessary to ensure that models for droplet vaporization predict vaporization rates with adequate accuracy under all conditions.

In this work we address the question: Is the current simplified droplet vaporization models employed in multidimensional models adequate to capture vaporization rates and drop lifetimes? The key unknown variable in modeling the sprays is the droplet size. Hence, this work also focuses on modeling the outcomes of droplet collisions that lead to the computed sizes.

Summary of the Most Important Results

The Computational Model

Studies are carried out with a detailed one-dimensional droplet vaporization model and a simplified droplet vaporization model as employed in multidimensional models [5-7] to obtain the results shown here and arrive at the conclusions.

The One-Dimensional Droplet Vaporization Model

The governing equations for the model are the conservation equations for mixture mass, internal energy and species for both the gas and liquid phases with additional relations for the flux terms contained therein [8]. To simplify the problem, the following assumptions are made here:

- A1: Droplet vaporization is spherically symmetric.
- A2: All non-radial velocities and fluxes are zero.
- A3: Fick's and Fourier's laws for mass and energy diffusion are used.
- A4: Energy terms arising from viscous dissipation, radiation, interdiffusion, and flow work are neglected.
- A5: Negligible Soret and Dufour effects.
- A6: Pressure is uniform and constant throughout.
- A7: Thermal, mechanical, and chemical equilibrium at the vapor/liquid interface.
- A8: Lewis and Raoult's assumptions are valid at the vapor/liquid interface.

With assumptions A1 through A6, the conservation equation for mixture mass in both the gas and liquid phase is:

$$\frac{\partial \rho}{\partial t} + \frac{1}{r^2} \frac{\partial}{\partial r} (r^2 \rho u_r) = 0 \quad (1)$$

and the conservation equation for mixture internal energy for the gas and liquid phase is:

$$\frac{\partial (\rho U)}{\partial t} + \frac{1}{r^2} \frac{\partial}{\partial r} (r^2 \rho U u_r) = \frac{1}{r^2} \frac{\partial}{\partial r} \left(\frac{k}{C_v} \frac{\partial}{\partial r} (r^2 U) \right) \quad (2)$$

and the conservation of species equation is

$$\frac{\partial (\rho Y_i)}{\partial t} + \frac{1}{r^2} \frac{\partial}{\partial r} (r^2 \rho Y_i u_r) = \frac{1}{r^2} \frac{\partial}{\partial r} \left(\rho D_i \frac{\partial}{\partial r} (r^2 Y_i) \right) \quad (3)$$

where ρ is the mixture density, k is the mixture thermal conductivity, C_v is the constant volume specific heat capacity, D_i is mass diffusivity of species "i", u_r is the radial velocity, U is specific mixture internal energy, and Y_i is the species mass fraction.

In addition, the integral forms of the conservation relations for mixture mass, energy, and species are applicable for a control volume which is situated on the vapor/liquid interface. In the limit as this control volume becomes infinitesimally thin about the interface the contributing terms of the flux components within the plane of the interface become negligible as compared to those normal to the interface. Therefore, accounting for the motion of the vapor/liquid interface, conservation of mass across the interface yields:

$$\dot{m}_{ls} = \rho_{ls}(u_{ls} - V_s) = \dot{m}_s = \rho_{gs}(u_{gs} - V_s) = \dot{m}_{gs} \quad (4)$$

where ρ_{ls} and ρ_{gs} are the liquid and gas phase mixture densities, u_{ls} and u_{gs} are the liquid and gas phase bulk velocities, and \dot{m}_{ls} and \dot{m}_{gs} are the rates of liquid and gas phase mass flux with all values being evaluated at the surface and V_s is the interface velocity.

Conservation of energy across the interface yields:

$$\dot{q}_{ls} = \dot{m}_s \Delta H_{vs} + \dot{q}_{gs} \quad (5)$$

where \dot{q}_{ls} is the energy flux in the liquid phase, \dot{q}_{gs} is the energy flux in the gas phase, and ΔH_{vs} is the enthalpy of vaporization (i.e., the enthalpy change across the interface) with all values being evaluated at the surface.

And, conservation of species across the interface yields:

$$\begin{aligned} \dot{m}_{ls(i)} &= \rho_{ls} Y_{ls(i)} (u_{ls} + V_{ls(i)} - V_s) = \dot{m}_{s(i)} \\ \dot{m}_{gs(i)} &= \rho_{gs} Y_{gs(i)} (u_{gs} + V_{gs(i)} - V_s) = \dot{m}_{s(i)} \end{aligned} \quad (6)$$

where the new variables $V_{ls(i)}$ and $V_{gs(i)}$ are liquid and gas phase diffusion velocities and $\dot{m}_{ls(i)}$ and $\dot{m}_{gs(i)}$ are the rates of liquid and gas phase mass flux of species "i" with all values being evaluated at the surface.

From assumptions A7 and A8, the following interface boundary conditions also apply:

$$T_{ls} = T_s = T_{gs} \quad (7)$$

$$p_{ls} = p_s = p_{gs} \quad (8)$$

$$X_{gs(i)} = X_{ls(i)} = \frac{p_{v(i)}(T_s)}{p_s} \quad (9)$$

where T_s is the surface temperature, p_s is the surface pressure, and $X_{ls(i)}$ and $X_{gs(i)}$ are the mole fractions of species "i" in the liquid and gas phases at the surface, respectively.

Full account of property variations with respect to pressure, temperature, and composition have been included within the model.

The finite-difference/finite-volume methods of Patankar [9] are used to solve Eqs. (1)-(9). The essence of the method involves breaking up the physical domain into a finite set of points for which at each point there is a prescribed volume in space, the control volume, containing the point. Upon assuming that the dependent variable in question behaves in a constant or linear fashion throughout the control volume, the conservation equations are integrated over each control volume to obtain algebraic relations in terms of the unknowns. The algebraic equations form a system of non-linear, coupled set of equations which are then solved in an iterative fashion. In the case of one dimension, the solution may be obtained in one application of the well-known tri-diagonal matrix algorithm method. However, due to nonlinearities arising from velocity, temperature, pressure, composition dependent properties, and fully implicit treatment of boundary conditions, repeated application of the solution process is implemented until a converged solution has been obtained.

Simplified Droplet Vaporization Model

In the simplified droplet vaporization model, the rate of change of mass of the droplet is given by the Frossling correlation [6-8].

$$-\frac{1}{3r_d^2} \frac{d}{dt} (\rho_\ell r_d^3) = \frac{(\rho D)_g}{r_d} B \frac{Sh_d}{2} \quad (10)$$

The rate of change of energy of the droplet is given by the equation:

$$\rho_\ell \cdot \frac{4}{3} \pi r_d^3 \frac{d}{dt} (C_\ell T_d) = \rho_\ell \cdot 4 \pi r_d^2 \frac{d}{dt} L(T_d) \frac{d}{dt} (\rho_\ell r_d^3) + 4 \pi r_d^2 \dot{Q}_d \quad (11)$$

$$B = \frac{Y_{vs} - Y_v}{1 - Y_{vs}}$$

$$\dot{Q}_d = \frac{\lambda_g (T - T_d)}{2r_d} \cdot Nu_d$$

In the equations above, r_d is the droplet radius, ρ_ℓ is the liquid density, D is the mass diffusivity of the gas, B is the transfer number, Sh_d is the Sherwood number, C_ℓ is the liquid specific heat, T_d is the droplet temperature, $L(T_d)$ is the latent heat of vaporization of the

liquid, \dot{Q}_d is the rate of heat conduction to the droplet, Y_{vs} is the droplet surface mass fraction of the fuel, Y_v is the mass fraction in the gas and given as $Y_v = \rho_u / \rho$, λ_g is the thermal conductivity of the gas and Nu_d is the Nusselt number.

The following additional correlations are employed to solve these equations:

$$Sh_d = \left(2.0 + 0.6 Re_d^{1/2} Sc_d^{1/3} \right) \frac{\ell n(1 + B)}{B}$$

$$Nu_d = \left(2.0 + 0.6 Re_d^{1/2} Pr_d^{1/3} \right) \frac{\ell n(1 + B)}{B}$$

$$Sc_d = \frac{\mu_g}{(\rho D)_g}$$

$$Pr_d = \frac{\mu_g C_{pg}}{\lambda_g}$$

$$Re_d = \frac{2\rho_d \left| \bar{u}_g + u'_g - u_d \right| r_d}{\mu_g}$$

$L(T_d)$ is obtained from the Haggenmacher correlation [7]

$$L(T_d) = \frac{R T_d^2}{W_v P} \left(\frac{dp}{dt} \right) \beta$$

where R is the universal gas constant, W_v is the molecular weight of the fuel, P is the vapor pressure of the fuel and β is the compressibility factor given by

$$\beta = \left[1 - \frac{T_c^3 p}{T^3 p_c} \right]^{1/2}$$

where T_c and p_c are critical values of temperature and pressure for the fuel. We have used the Atoine equation to obtain the vapor pressure [10]

$$\log_{10} p = A - \frac{B}{T + C}$$

where the constants A, B and C may be obtained for the fuel.

The properties $(\rho D)_g, \mu_g, \lambda_g$ are evaluated at a mean temperature, \hat{T} , obtained using the 2/3 law [6, 11].

$$\hat{T} = \frac{T_g + 2 T_d}{3}$$

The simplified droplet vaporization model, described above, is also capable of modeling multicomponent droplet vaporization. The multicomponent droplet vaporization model has been developed with support from the ARO [12].

It has been shown in detailed numerical studies of isolated multicomponent droplets that the two important controlling physical processes, which determine the rate at which one component vaporizes relative to another, are the volatility of the component as reflected, in part, in its latent heat of vaporization and the inter-species liquid diffusivity of the component. The greater the volatility and the lower the latent heat of vaporization of the component, the faster it vaporizes. The greater the inter-species liquid diffusivity of the component in a multicomponent mixture, the faster it diffuses to the surface of the droplet and the faster it vaporizes. Our model is built on these essential physics. Consider the physical picture, as shown in Fig. 1(a), of an N-component liquid droplet of radius R, with the species mass fractions of $Y_{l,i}, i=1, \dots, N$, in an ambient environment of temperature T_a , pressure P_a and vapor species $Y_{v,a}, i=1, \dots, N$. There is a heat flux of Q into the droplet of which Q_v is utilized to vaporize the component and Q_l to heat the droplet. There are two important characteristic times which then control the vaporization process of each species: $\tau_{v,i}$ is the characteristic time associated with the vaporization of the individual species with the more volatile species having a shorter time and the less volatile one having a longer time. $\tau_{d,i}$ is the characteristic time associated with the inter-species liquid diffusivity of species I in the multicomponent mixture. The model is developed as follows: At any instance in time, as shown in Fig. 1(b), we assume that there are N droplets each of a single component species I, radius R and the same ambient environment as the multicomponent droplet at the instance in time. The heat flux to each of the single component droplet is assumed to be the same as the heat flux to the multicomponent droplet. A vaporization rate, $\dot{m}_{v,i}$, for each single component droplet and hence each component may then be evaluated using the mass and energy balance equations discussed earlier.

The rate of vaporization of any component in the multicomponent droplet, $\tilde{m}_{v,i}$, would be different from the value computed for this single component droplet, $\dot{m}_{v,i}$, since the concentration of the species on the surface of the multicomponent droplet will be different from 1.0. the actual vaporization rate of the species in the multicomponent droplet is modeled as

$$\tilde{m}_{v,i} = \dot{m}_{v,i} \tilde{Y}_{l,i} \quad (12)$$

where $\tilde{Y}_{l,i}$ is the actual component mass fraction on the surface of the multicomponent droplet. $\tilde{Y}_{l,i}$ will depend on the liquid-phase diffusivity of the species I with the species which has a greater diffusivity likely to have a higher concentration on the surface. This is modeled in the second of the two essential elements as

$$\tilde{Y}_{l,i} = Y_{l,i} \frac{D_{l,i}}{\left[\sum_{j=1}^N D_{l,j} Y_{l,j} \right]} \quad (13)$$

where $Y_{l,i}$ is the mass fraction species I in the multicomponent droplet and $D_{l,i}$ is the effective diffusivity of species I in the mixture. The physical picture represented here is that the concentration of the more diffusive species will be greater at the surface than that of the less diffusive one and hence more of it will vaporize. In this manner the effects of volatility and species diffusion are modeled.

For the liquid-phase diffusivity of each component, we have used the Wilke-Chang equation for the effective diffusivity, $D_{l,i}$, of each component [10]

$$D_{l,i} = 7.4 \times 10^{-8} \frac{(\Phi M)^{\frac{1}{2}} T}{\eta_i} V_i^{0.6} \text{ cm}^2/\text{s} \quad (14)$$

where

$$\Phi M = \sum_{j=1, j \neq i}^N x_j \Phi_j M_j \quad (15)$$

In the equation above, x is the mole fraction of the component in the liquid droplet, M is the molar mass, V is the molar volume, Φ is the association parameter for the solvent and η is the viscosity. η_i is obtained from the Grunberg-Nissan equation [10]:

$$\ln \eta_i = \sum_{i=1}^N x_i \ln \eta_i + \frac{1}{2} \sum_{i \neq j} \sum_{j=1}^N x_i x_j G_{ij} \quad (16)$$

where G_{ij} is an interaction parameter which is a function of the components I and j and the temperature T. We include temperature dependent properties for the liquid phase density, conductivity, specific heat capacity, viscosity and latent heat of formation.

In the numerical calculation procedure, the equations for droplet mass and energy transfer are applied to each of the N droplets, where each droplet is of a single component of the N components, at each step and individual vaporization rates are computed. In the case of a droplet reaching the critical state, it is assumed to vaporize completely at that point. Once the individual vaporization rates are known then the weighted vaporization rates for the components in the multicomponent droplet may be computed. An energy and mass balance for the multicomponent droplet then leads to updated values of temperature and composition and the procedure is then repeated.

These models were employed in three different geometries which are schematically illustrated in Fig. 2.

The computational grids employed for the detailed droplet computation, the single droplet computation using the multidimensional model and the spray computations using the multidimensional model are shown in Figs. 2(a), (b) and (c) respectively. Figures 2(a) and (b) are schematics.

Computations have been performed for single droplets of the pure components *n*-hexadecane, *n*-tetradecane, *n*-hexane, and benzene vaporizing in quiescent environments initially at a uniform temperature, pressure, and composition. Table 1 lists the critical constants of these species. In all studies performed here, the initial droplet temperature was uniform at 300 K and initial droplet diameters were 30 μm or 245 μm .

The Combustion Submodel

The combustion submodel, that is employed here, includes a model for predicting autoignition and one for computing the subsequent combustion of the ignited gas. Our high-temperature combustion model follows the evolution of N fuel species and six additional species, O_2 , N_2 , CO_2 , H_2O , H_2 and CO , by solving the follow with i -th species conservation equation together with all other flow and spray equations

$$\frac{\partial Y_i}{\partial t} + v_j \frac{\partial Y_i}{\partial x_j} = - \frac{1}{\rho} \frac{\partial \rho_i}{\partial x_j} V_{ij} = \dot{w}_i \quad (17)$$

In the above equation, Y_i is the mass fraction of species i , v_j is the velocity in the direction j , x_j is the distance in the direction j , ρ is the gas density, V_{ij} is the diffusion velocity of species i in the direction j , and \dot{w}_i is the rate of formation of species i . The rate of change of species partial density is given by the expression

$$\frac{d\rho_i}{dt} = - \frac{(\rho_i - \rho_i^*)}{\tau_c} \quad (18)$$

where ρ_i^* is the local and instantaneous equilibrium value of the i -th species. τ_c is a characteristic time with which the equilibrium is attained. It is obtained from the following expression:

$$\tau_c = \max(\tau_t, \tau_l) \quad (19)$$

where τ_t is a turbulent eddy turnover time and τ_l is the characteristic time with which the equilibrium is achieved in a laminar flame. τ_l is obtained by comparing experimental and computed laminar flame speeds. In extending this model to multiple fuel components, the local value of the fuel density is taken to be the sum of the partial densities of the different components. In computing the local and instantaneous equilibrium species densities, we consider the fuel species as a composite one with the formula $C_xH_yO_z$ where the local values of x , y and z may be determined from the local concentrations of the individual fuel species.

To model autoignition, we add to the 6+N species a new species that represents the evolution of the radicals that lead to ignition. The evolution of this additional species is controlled again, like that of the others, by convection diffusion and chemical formation. However, this species is assumed to be a trace species and hence no mass is associated with it. In our previous work, where we considered only one fuel species, the chemical formation was due only to that species. In this work, where we have more than one species in the multicomponent fuel, the different fuel species will contribute to the formation of this trace species and at different rates. In our model, we assume that the activation temperature in the rate expression that yields the trace species from each component is inversely proportional to the cetane number, CN, of the component [13,14]. The model for the species is then Eq. (17) and the following equations

$$V_{m,k} = - \left(D_e \frac{\partial Y_m}{\partial x_k} \right) / U_m \quad (20)$$

$$\dot{w}_m = \sum_{i=1}^N \frac{1}{\tau_{m,i}} \quad (21)$$

$$\tau_{m,i} = \left[A \left(\frac{P}{P_o} \right)^B \right] e^{d(1+C|1-\phi|)/(T(CN)_i)} \quad (22)$$

where D_e is the effective diffusivity, i.e., the sum of the laminar and turbulent diffusivities, P is the pressure in atm, T is the gas temperature in K, ϕ is the equivalence ratio and A , B , C , D are constants that are determined by comparisons with measured ignition delay times.

Discussion of Results

Results from the simplified and detailed vaporization models are shown in Figs. 3 and 4 for single component droplet. The results are for single component hexadecane droplets. Figure 3 shows results for the computation where the ambient pressure is 10 atm and ambient temperatures of 600 K and 900 K are selected. These temperatures encompass the cold start operating range. Figure 3 shows that the simplified model reproduces the size history of the drops and the lifetime of the drop within 15% for these conditions.

When the ambient pressure is increased to 50 atm Fig. 4 shows that the maximum differences in life history and drop lifetime are still within 15%. This implies that, for these conditions, the simplified droplet vaporization model predicts the vaporization characteristics with adequate accuracy. Figure 5 shows the drop surface and mass averaged drop temperature as a function of time. Provided these temperatures are within 50 K of each other, the simplified vaporization model reproduced the detailed results with adequate accuracy. This is certainly the case for droplets in Diesel engines under cold start conditions. Figure 6 shows the size history of a droplet at an ambient temperature of 1300 K and pressure of 50 atm. In this case the differences in lifetime is about 50%. Figure 7 shows the surface temperature and mass averaged drop temperature for the droplet under these conditions. Significant differences between the two temperatures may be observed. In this case, the simplified vaporization model is not adequate. However, under these conditions corresponding to warm operating conditions in a turbocharged engine under heavy load, the liquid vaporization and penetration is controlled by mixing rates and not by the rate of droplet vaporization. This has been shown experimentally by [15] and computationally [4, 16].

As part of this work, the conditions under which droplets reach the critical state in a Diesel engine have also been investigated. This topic is important, in part, because simplified vaporization models are unlikely to reproduce near-critical vaporization with adequate accuracy.

Figure 8 shows the effect of ambient temperature on droplet size for a constant ambient gas pressure of 50 atm. The normalized droplet diameter squared has been plotted as a function of the scaled time for a n-hexadecane droplet vaporizing in nitrogen at ambient temperatures of 600, 700, 800, 1000, and 1300 K. the expected trend of reduced droplet lifetime with increasing ambient temperature is reproduced. At ambient temperatures of 800 K and below and after an initial transient period, the droplet exhibits the well-known D-squared vaporization regime over a significant portion of its lifetime even at this relatively high ambient pressure. However, this behavior is not reproduced at higher temperatures. Figure 9 shows the normalized droplet diameter squared as a function of the scaled time for the ambient temperature of 1300 K and ambient pressure of 50 atm. It may be seen that there no longer appears to be a well-defined D-squared vaporization regime throughout the droplet's history.

Figure 10 shows the corresponding droplet surface temperatures for the conditions considered in Fig. 2. it may be seen that for an ambient temperature of 600 K the droplet surface temperature attains the pseudo wet-bulb state for a significant portion of the droplet's lifetime. However, at an ambient temperature of 1300 K the droplet surface temperature is entirely transient and, in fact, reaches the critical point near the end of its lifetime. Under these ambient

conditions of $P=50$ atm and $T=1300$ K, the quasi-steady theory would appear to no longer apply as seen in both the droplet's size and surface temperature histories.

Figure 11 shows the loci of lowest ambient reduced temperature (± 10 K) at a fixed reduced pressure which results in the droplet surface reaching the critical temperature of the pure component species. Here, the ambient temperatures and pressure have been reduced by the critical temperatures and pressures of the liquid species. The critical loci shown for n-hexadecane and n-tetradecane are in qualitative agreement with previous suggestions [17] that vaporizing pure component droplets will reach the critical state when reduced ambient pressures are greater than 2.0 and reduced ambient temperatures are greater than 2.0. In fact, this figure shows that for these pure component droplets, when either reduced ambient pressure or reduced ambient temperature is greater than 2.0, the value of the other at which the droplet reaches the critical state may be less than 2 and its value will decrease as the value of the other increases. Figure 11 also shows that the critical loci is fuel dependent.

The departure of the critical loci for n-hexane and benzene from that of n-hexadecane and n-tetradecane may be due to the much greater critical pressures for the former two species, 30.3 and 48.9 atm, as compared to the latter two species, 13.3 and 14.4 atm, respectively for the same reduced pressure, the high critical pressure species will be vaporizing in an ambient gas which is at a much greater pressure than the low critical pressure species. As a result, the mass diffusion rates will be reduced with a corresponding reduction in mass vaporization rates. Since mass vaporization is the means by which the droplet carries away the energy flux to its surface, droplet heating is enhanced for these high critical pressure species and the droplet will be more likely to reach the critical point at a lower reduced ambient temperature. This reasoning would also explain why the critical loci for benzene is lower than that of n-hexane.

Figure 12 shows a comparison of the critical loci for n-hexadecane droplets vaporizing in pure nitrogen and carbon dioxide environments. Above a reduced pressure of approximately 2.5, there is essentially no change in the critical loci. However, below this pressure the critical loci for vaporization in carbon dioxide lies below that of nitrogen. Thus for pressures below 35 atm, this suggests that a vaporizing droplet may reach the critical point at a lower ambient temperature if the ambient gas contains significant amounts of carbon dioxide. This may again be related to differences in the mass diffusion rates of the two species, as explained in the previous paragraph, leading to more effective droplet heating in the case of the carbon dioxide ambient gas.

Now, we ask the question: Do multidimensional vaporizing spray models that are in widespread use today [6-7] reproduce the trends identified above? In today's production Diesel engines, it may appear unlikely that the compression temperatures reach the values that should result in the droplet reaching the critical point. Also, vaporization of the liquid will result in the cooling of the cylinder gas. Hence, droplets are likely to reach the critical point only if they are within the reaction zones. Experimental results, however, do not support this possibility of drops being in the reaction zone [18].

To answer the question posed above, next, we present results from computations where we employ the multidimensional model [7] to perform single droplet vaporization computations.

The single droplet is assumed to be at rest in an ambient which is also at rest initially. Figure 1(b) shows a schematic of the computational domain. The gas void fraction is close to one in the computational cell. The liquid species is tetradecane. Figure 13 shows the variation of the computed normalized diameter of the drop with time for four cases when the temperature is held constant at 1400 K but the ambient pressures are 20 atm, 32 atm, 48 atm and 68 atm. The initial ambient density is kept fixed at 16.67 kg/m^3 . This is achieved by changing the molecular weight of the ambient gas. 1400 K, in the case of tetradecane, corresponds to $T_r = 2.02$. The corresponding P_r for the four cases are 1.39, 2.2, 3.33 and 4.72. On the figures, the abrupt transitions in radius results when the droplet reaches a critical state. It may be seen that at $P_r = 1.39$, the droplet vaporizes completely without reaching the critical state. However, as the pressure is increased, the droplet reaches the critical state at earlier stages in its vaporization. As the pressure is raised, the vaporization rate decreases and the self-cooling of the droplet is not sufficiently rapid to avoid the temperature reaching the critical value. It is interesting to observe that the model predicts that this critical state is achieved at about the same time in all cases. This appears to result from a balance between the net rate of heat transfer to the droplet, which increases as the pressure is raised, and the greater mass of the droplet whose temperature has to be changed at any given time as a result of slower vaporization. These results are consistent with those from the detailed computations presented earlier. Figure 14 shows the variation of the computed normalized diameter of the drop with time for three cases when the pressure is held constant at 48 atm but the initial ambient temperatures are 992 K, 1200 K and 1400 K. The initial ambient density is again fixed at 16.67 kg/m^3 in all cases. 48 atm corresponds to $P_r = 3.33$ and the temperatures correspond to $T_r = 1.44$, 1.74 and 2.02. In this case, the droplet reaches the critical state at earlier times and at larger radius as the initial ambient temperature is raised. It is seen however that the droplet reaches a critical state even at $T_r = 1.44$. However, this may result because $P_r = 3.33$ rather than about 2.0 [17]. Figure 11 shows that at $P_r = 3.33$, T_r for the critical state to be reached is about 1.7. The important conclusion here is that under cold start conditions, droplets do not reach a critical state in a Diesel engine. The ambient conditions would have to correspond to about twice the critical pressure and about twice the critical temperature for the droplet to reach a critical condition. These conditions would correspond to warm operating conditions in a turbocharged engine under high load. However, as pointed out earlier, under such conditions the vaporization rate is mixing controlled and individual droplet vaporization is not relevant in Diesel sprays.

The single most important parameter that has to be known in order to predict the vaporization rates in a Diesel spray is the droplet diameter and this information is not available accurately in sprays as it depends on atomization, collisions and drop break-up. As part of the work carried out on this contract, a new algorithm that predicts the outcome of drop-drop collisions has been developed. The current model includes coalescence and grazing collisions as possible outcomes. The new model that has been developed includes bounce, reflexive separation, high-pressure effects and drop shattering as additional outcomes. Bounce, reflexive separation and high-pressure effects have been modeled to reproduce experimental results of [19]. The works of Estrade et al., and Ashgriz and Poo have also been employed to determine the different regimes on a Weber number-impact parameter plot. The model that has been developed is referred to as the composite collision model. Of these, bounce has been shown to

have a significant influence on the computed droplet sizes. The work is described in greater detail in reference [20].

Figure 15 shows the SMD of the drops in a cube ('box') where the drops are uniformly distributed as a function of time obtained by employing the Brazier-Smith et al. [21] model for coalescence efficiency. Results are presented for four resolutions. It may be seen that the results do not change significantly for resolutions greater than $40 \times 40 \times 1$. At 100 ms after start of computation, the SMD has increased from an initial value of $2 \mu\text{m}$ to $2.85 \mu\text{m}$, an increase of greater than 40%. Figure 16 shows the results when the composite coalescence model proposed here is employed and compares them with results from the model of Brazier-Smith et al. [21]. Results are presented for the same two resolutions where convergence is achieved. At 100 ms after start of computation, the SMD has increased to about $2.17 \mu\text{m}$ with the composite model, an increase of less than 10%, whereas it has increased to about $2.85 \mu\text{m}$ with the Brazier-Smith et al. [21] model, an increase of over 40%. Hence, the composite model predicts a noticeably lower coalescence efficiency relative to the Brazier-Smith et al. [21] model. The primary difference between the two models is the inclusion of sub-model for bounce, which reduces the tendency to coalesce.

We have also examined how the model for shattering collisions affects the computed outcomes [22]. Figure 17 shows results with the composite model when shattering collisions are not included and compares them to computations when we have allowed shattering to occur for collisions with $We > 100$ in one case and for $We > 1000$ for another case. The choice of these cutoffs for We are somewhat arbitrary and are meant to give insight into how shattering collisions might affect computed results. In the computations with shattering, shattering is only allowed to occur after a rotational or a reflexive separation has been predicted by the composite model. Shattering does not occur after a bouncing separating, since the drops do not actually touch during bouncing and the disruption of the drops' surfaces necessary for shattering does not occur. As can be seen in Fig. 17, there is negligible difference in results when shattering is allowed for $We > 1000$. This indicates that most of the collisions in this problem are at We lower than 1000. When shattering is predicted for $We > 100$ there is a larger difference initially as the drop size reduces by about 10%. The differences arise in the early stages of computation when the We numbers are larger and shattering is more dominant. As the initial turbulence in the box decays, the We of the collisions becomes lower and the drops stop shattering and coalesce. To assess the impact of the coalescence model on computed Diesel sprays, computations were carried out in the axisymmetric chamber described in the previous section.

Summary

1. A simplified droplet vaporization model that accounts for drop bulk temperature, heat and mass transfer effects has been shown to reproduce droplet size history with adequate accuracy compared to a detailed droplet vaporization model under cold-start conditions and warm operating conditions except under the high pressure ($P > 50 \text{ atm}$) and very high temperature ($T > 1200 \text{ K}$) conditions encountered in a Diesel engine.
2. It is shown that droplets reach a critical state of vaporization only under the high pressure and very high temperature conditions in the engine but certainly not under cold start conditions.

3. It is shown that under warm operating conditions in a Diesel engine vaporization is essentially mixing-controlled and the details of a droplet vaporization model are not relevant.
4. An improved model for predicting drop sizes in Diesel sprays that result from drop-drop collisions has been developed.

Table 1. Critical Constants of Pure Fluids

Fuel	T_c (K)	P_c (bar)
n-hexane	507.5	30.3
n-tetradecane	693.0	14.4
n-hexadecane	717	13.3
Benzene	562.2	48.9

1. PUBLICATIONS SUPPORTED UNDER THIS GRANT

(a) *Peer-Reviewed Journals*

1. V. Iyer, S. Post and J. Abraham, "Is the Liquid Penetration in Diesel Sprays Mixing Controlled?" *Proc. Combustion Institute*, 28: 1111-1118, 2000
2. J. Abraham and S.D. Givler, "Conditions in Which Vaporizing Fuel Drops Reach a Critical State in a Diesel Engine," *SAE Trans.*, 108: 601-612, 2000.
3. S. Post and J. Abraham, "A Computational Study of the Processes that Affect the Steady Liquid Penetration in Full-Cone Diesel Sprays," *Combust. Sci. Tech.*, 165: 1-20, 2001.

(b) *Conference Proceedings*

1. S. Post and J. Abraham, "Modeling the Liquid Penetration in Diesel Sprays," *Proc. of the 1st Joint Meeting of the U.S. Sections of the Combustion Institute*, 224-227, Washington, DC, March 1999.
2. S. Post and J. Abraham, "Challenges in Modeling the Liquid Penetration in Diesel Sprays," *Proc. Of the 12th Annual Conference on Liquid Atomization and Spray Systems*, 31-35, Indianapolis, May 1999.

(c) *Manuscripts Submitted*

1. S. Post and J. Abraham, "Modeling the Outcome of Drop-Drop Collisions in Sprays," *Int. J. Multiphase Flow* (revised), July 2001.

Scientific Personnel

Professor John Abraham

Professor Vinicio Magi (Visiting Professor from Italy)

Scott Post, Ph.D., 2001

Shawn Givler

Bibliography

1. Bracco, F., "Modeling of Engine Sprays," *SAE Trans.* 94, 144-167, 1985.
2. Aneja R. and Abraham, J., "How Far Does the Liquid Penetrate in a Diesel Engine: Computed Results vs. Measurements?" *Combustion Science and Technology*, 138, 233-256, 1998.
3. Post, S. and Abraham, J., "A Computational Study of the Processes That Affect the Steady Liquid Penetration in Full-Cone Diesel Sprays," *Combust. Sci. Tech.*, 165, 1-20, 2001.
4. Iyer, V.A., Magi, V. and Abraham, J., "Exploring Injected Droplet Size Effects on Steady Liquid Penetration in a Diesel Spray with a Two-Fluid Model," *Int. J. Heat and Mass Transfer*, to appear 2001.
5. Amsden, A.A., O'Rourke, P.J. and Butler, T.D. "KIVA-II: A Computer Program for Chemically Reactive Flows with Sprays," *Los Alamos National Laboratory Report No. LA-11560-MS*, 1989.
6. Abraham, J. and Givler, S.D., "Conditions in Which Vaporizing Fuel Drops Reach a Critical State in a Diesel Engine," *SAE Transactions*, 108, 601-612, 2000.
7. Magi, V., "REC-2000: A Multidimensional Code for Transient, Two-Phase, Turbulent Reacting Flows," *Engine Research Laboratory Report*, School of Mechanical Engineering, Purdue University.
8. Williams, F.A., *Combustion Theory*, Benjamin Cummings Publishing Co., Menlo Park, CA, 1985.
9. Patankar, S.V., *Numerical Heat Transfer and Fluid Flow*, Hemisphere Publishing Co., New York, 1980.
10. Reid, R.C., Prausnitz, J.M. and Poling, B.E., *The Properties of Gases and Liquids*, McGraw-Hill, Inc., 4th Ed., 1987.
11. Hubbard, G.L. Denny, V.E. and Mills, A.F., "Droplet Evaporation: Effects of Transients and Variable Properties, *Int. J. Heat Mass Transfer*, 18, 1003-1008, 1975.
12. Abraham, J. and Magi, V., "A Model for Multicomponent Droplet Vaporization in Sprays," *SAE Transactions*, 107, 603-613, 1999. Also in *Diesel Combustion Processes*, SP-1328, 117-128, SAE, Warrendale, PA, 1998.

13. Hardenberg, H.O. and Hase, F.W., "An Empirical Formula for Computing the Pressure Rise Delay of a Fuel From Its Cetane Number and From the Relevant Parameters of Direct-Injection Diesel Engines," *SAE Paper 790493*, 1979.
14. Olree, R.M. and Lenane, D.L., "Diesel Combustion Cetane Number Effects," *SAE Paper 840108*, 1984.
15. Siebers, D.L., "Liquid-Phase Fuel Penetration in Diesel Sprays, *SAE Paper 980809*, 1998.
16. Iyer, V., Magi, V., and Abraham, J., "Exploring Injected Droplet Size Effects on Steady Liquid Penetration in a Diesel Spray with a Two-Fluid Model," to appear in *Int. J. Heat and Mass Transfer*, 2001.
17. Givler, S.D. and Abraham, J. "A Review of Supercritical Droplet Vaporization and Combustion Studies," *Prog. Energy, Combust. Sci.*, Vol. 22, 1-28, 1996.
18. Dec. J., "A Conceptual Model of DI Diesel Combustion Based on Laser-Sheet Imaging," *SAE Paper 970873*, 1997.
19. Qian, J. and Law, C.K., "Regimes of Coalescence and Separation in Droplet Collision," *J. Fluid Mech.* 331, 59-80, 1997.
20. Post, S.L. and Abraham, J., "Modeling the Outcome of Drop-Drop Collisions in Diesel Sprays," submitted (revised) to *Intl. J. Multiphase Flow*, July 2001.
21. Brazier-Smith, P., Jennings, S. and Latham, J., "The Interaction of Falling Rain Drops: Coalescence," *Proc. R. Soc. Lond.*, A 326, 393-408, 1972.
22. Georjon, T.L. and Reitz, R.D., "Drop-Shattering Collision Model for Multidimensional Spray Computations," *Atomization and Sprays* 9, 231-254, 1999.

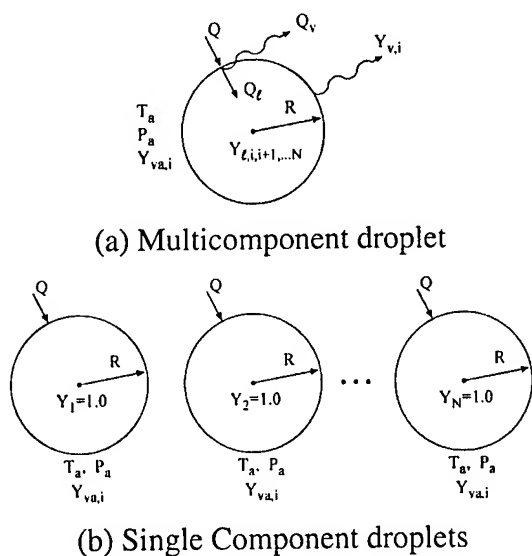


Fig. 1. Schematic of model formulation.

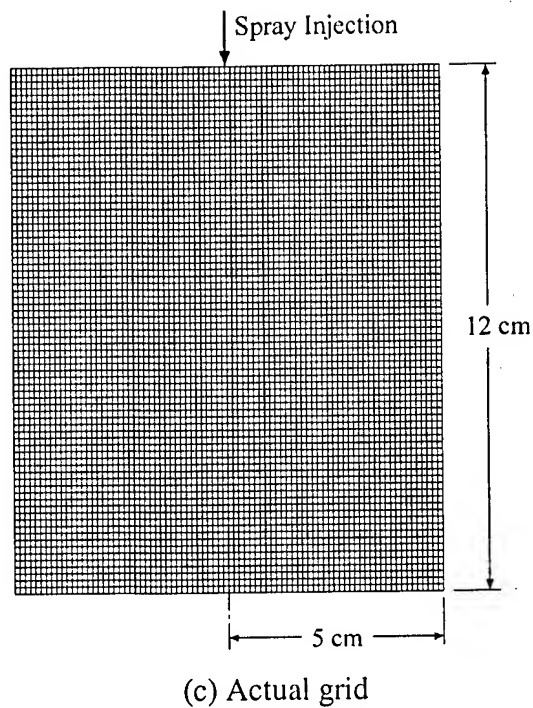
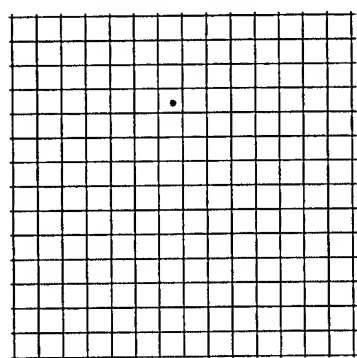
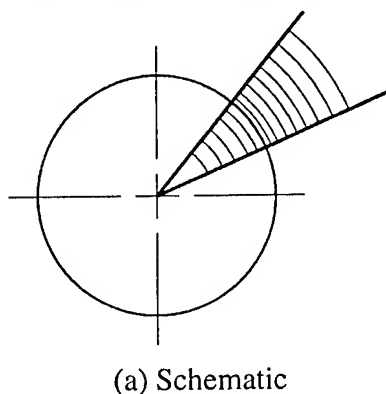
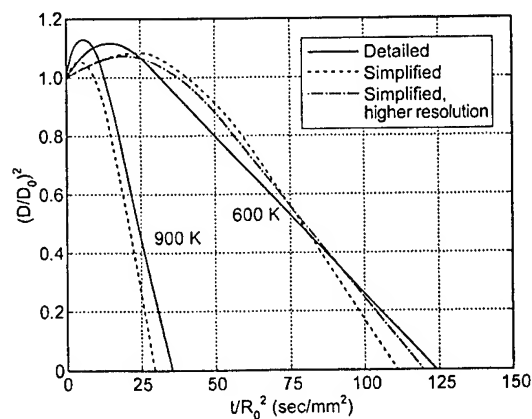


Fig. 2. Computational domain and grid for (a) detailed single droplet, (b) single droplet employing multidimensional model and (c) multidimensional spray computations.



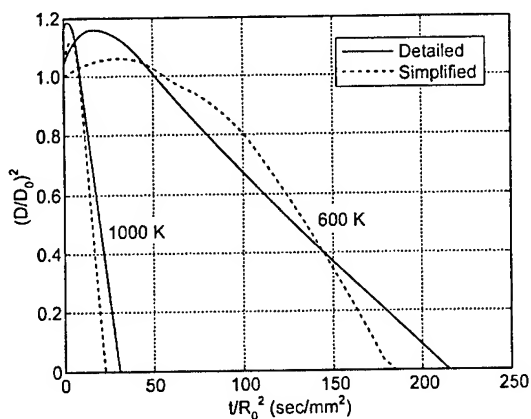


Fig. 4. Size histories of n-hexadecane droplets.

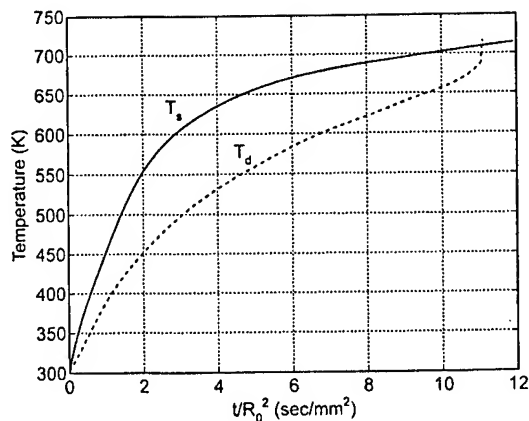


Fig. 7. Drop temperature as a function of time.

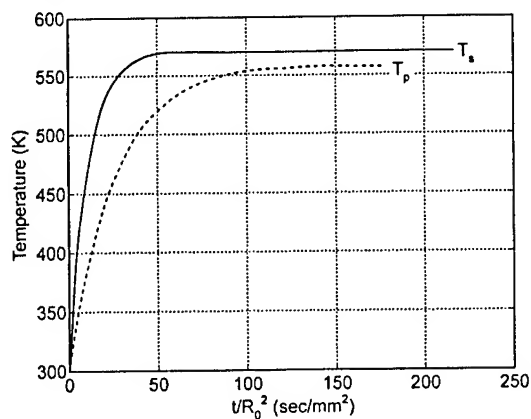


Fig. 5. Drop temperature as a function of time.

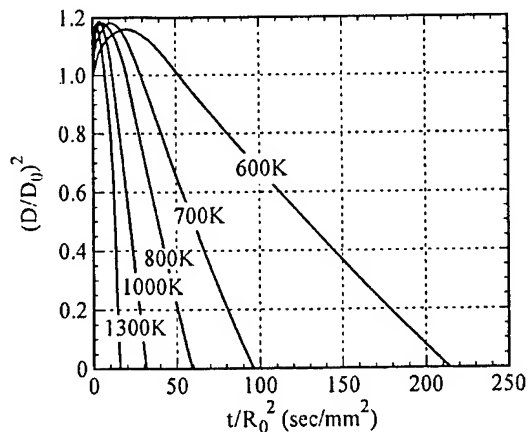


Fig. 8. Size histories of n-hexadecane droplets vaporizing in nitrogen at 50 atm.

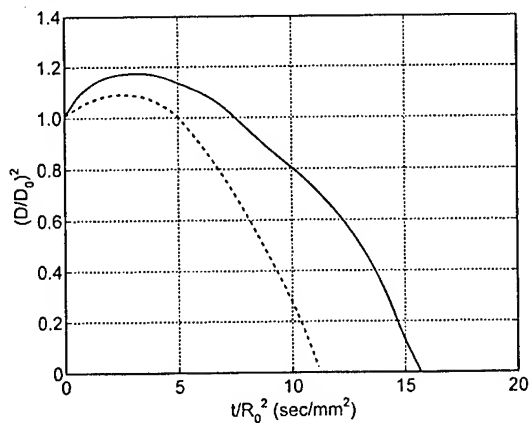


Fig. 6. Size history of n-hexadecane droplet.

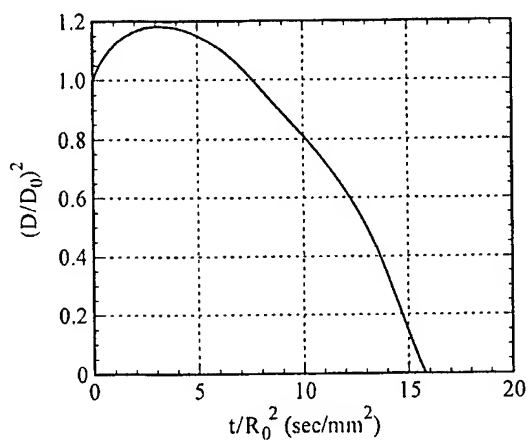


Fig. 9. Size history of n-hexadecane droplet vaporizing in nitrogen at 50 atm and 1300K.

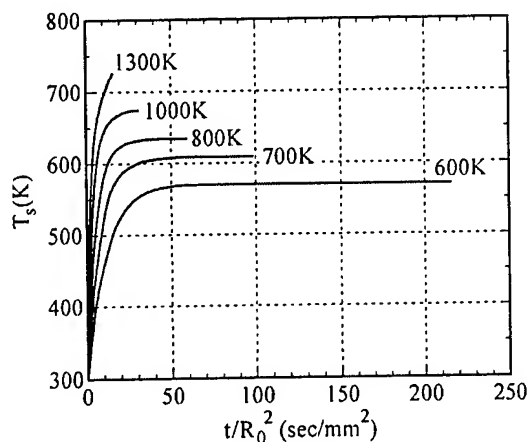


Fig. 10. Surface temperatures of n-hexadecane droplets vaporizing in nitrogen at 50 atm.

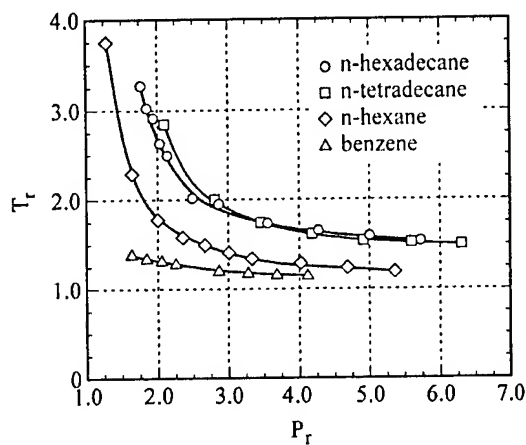


Fig. 11. Critical loci for droplets vaporizing in nitrogen environments.

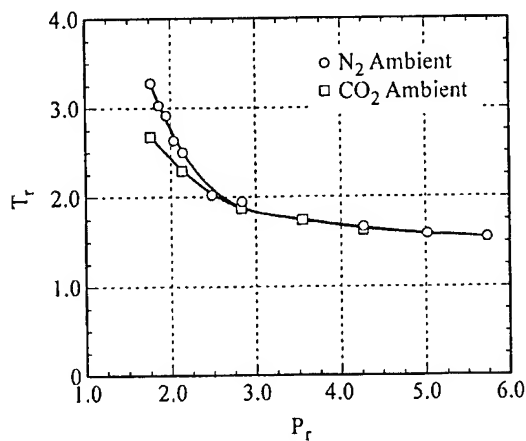


Fig. 12. Normalized mass vaporization rate of a 245 mm C6/C16 (50/50 by mass) droplet vaporizing in nitrogen.

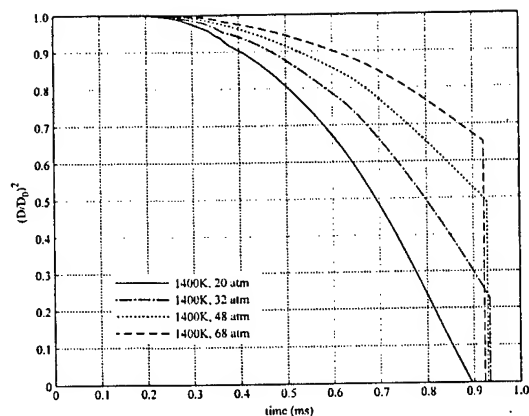


Fig. 13. Variation of drop size with time for droplet in ambient with same initial temperature of 1400K but different pressures.

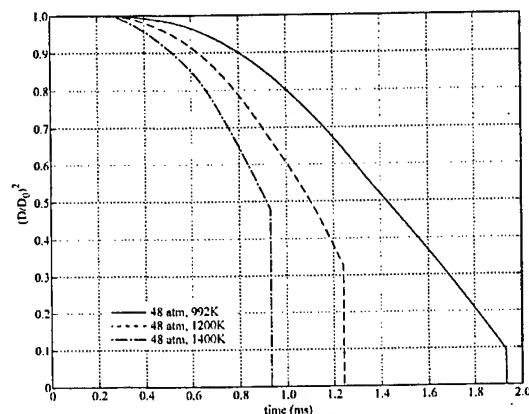


Fig. 14. Variation of drop size with time for droplet in ambient with same initial pressure of 48 atm but different temperatures.

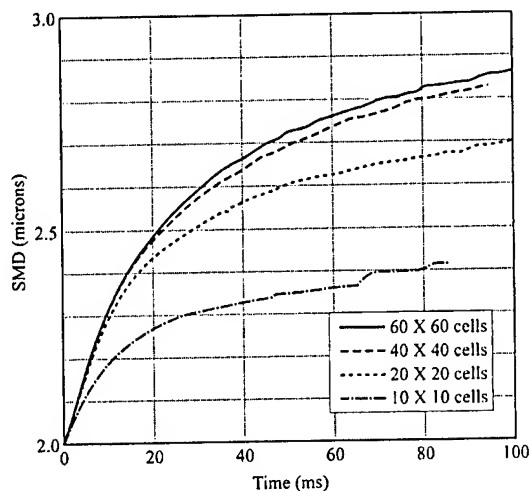


Fig. 15. Computed SMD for 10,000 parcels uniformly distributed throughout a $5 \times 5 \times 0.5$ cm domain at 300K, 1.16 kg/m^3 . 1000 drops per parcel. Brazier-Smith et al. (1972) coalescence model employed.

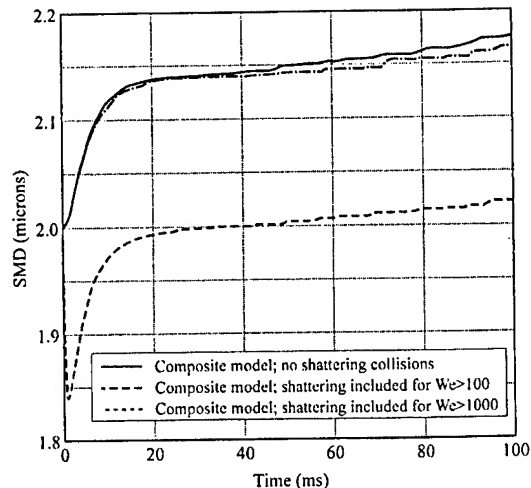


Fig. 17. Computed SMD for 10,000 parcels uniformly distributed throughout a $5 \times 5 \times 0.5$ cm domain at 300K, 1.16 kg/m^3 . 100 drops per parcel. Grid resolution is 40×40 cells.

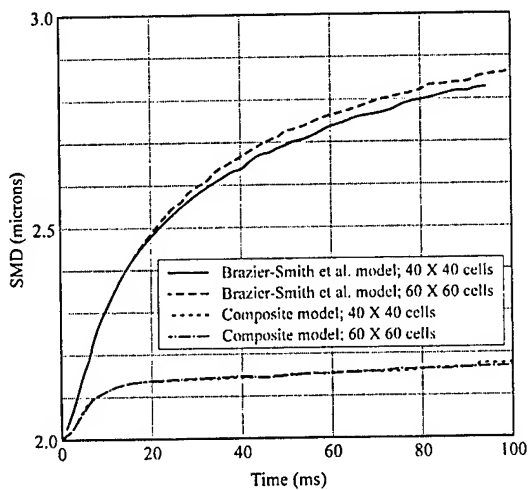


Fig. 16. Computed SMD for 10,000 parcels uniformly distributed throughout a $5 \times 5 \times 0.5$ cm domain at 300K, 1.16 kg/m^3 . 100 drops per parcel. Brazier-Smith et al. (1972) and composite models are compared.